Journal of Manufacturing Processes xxx (2015) xxx–xxx

Contents lists available at ScienceDirect

Journal of Manufacturing Processes

journal homepage: www.elsevier.com/locate/manpro

Technical Paper

The dynamics of laser surface modification

C. Earl[a,b], J.R. Castrejón-Pita[c,*], P.A. Hilton[b], W. O'Neill[a]

[a] Centre for Industrial Photonics, Department of Engineering, University of Cambridge, 17 Charles Babbage Road, Cambridge CB3 0FS, UK
[b] TWI Ltd, Granta Park, Great Abington, Cambridge CB21 6AL, UK
[c] School of Engineering and Material Science, Queen Mary University of London, Mile End Road, London E1 4NS, UK

ARTICLE INFO

Article history:
Received 26 May 2015
Accepted 6 October 2015
Available online xxx

Keywords:
Laser processing
Manufacturing
Fluid mechanics

ABSTRACT

The mechanisms involved in the production of surface features of protruding material formed by the interaction of a laser beam and a metallic substrate are investigated aiming to optimise the process efficiency. A relationship between laser induced surface features and filament breakup theory has been established. Results indicate that for the production of features the geometry of the protrusion with a filament critical aspect ratio over 6.0 ± 1.0 is required. In addition results show the surface tension, viscosity and density of the molten material, and the dynamics of the process dictate the characteristics of the forming feature. Using filament breakup and spatter production equations surface feature processing parameters can be predicted as demonstrated by the three metallic materials used in this study: Aluminium 5000 series, Stainless steel 304 and Ti–6Al–4V, all of which show consistent results.

1. Introduction

1.1. Background

Surface modification is of interest for potential applications to fields requiring an increased surface area; examples include material bonding and heat exchange. One such solution is Surfi-Sculpt® invented by TWI Ltd. [1], this surface modification technique uses repeated swipes of an electron or laser beam to produce surface features on material surfaces. The laser beam process variant involves translating a power beam source across the surface of the substrate in a manner similar to keyhole welding. This melts the material and causes the liquid to flow in the opposite direction to beam translation. Repeated swipes enable a protruding feature to be produced with a corresponding intrusion on the material, Fig. 1a. A range of forms can be easily produced by modifying the processing parameters, such as the laser power, the speed of translation or the number of swipes, as shown in Fig. 1b.

Traditionally, this surface modification technique has been thought to have been caused only by the surface tension of the molten material [2,3]. More recently, other mechanisms have also been considered, such as the fluid dynamics driven by a laser-induced thermo-capillary [4]. In this paper, high-speed imaging has been used to show that a protruding liquid filament (jet) is produced in response to the laser power and translation speed, which in turn solidifies producing a material feature. It is therefore thought that the surface feature production mechanism is dependent on the stability of the liquid filament of molten material. If the filament breaks up, producing spatter, then the material can no longer be utilised for feature production. In this work on the initial laser swipe, it is demonstrated that both the surface tension and the dynamics in a laser induced keyhole in the bulk of the material are responsible for the feature characteristics.

1.2. Keyhole dynamics

The dynamics of the melt flow in the pool within the keyhole are complex and depend on many mechanisms. The keyhole is formed due to the ablation recoil pressure induced by the vaporisation of the substrate material, which exceeds hydrostatic and surface tension forces of the surrounding material [5]. The recoil pressure compresses the metallic liquid generated on the keyhole front causing it to move around the keyhole towards the rear of the melt pool [6]. Keyholes occur at processing intensities over 10^6 W cm^{-2}, when the melt's vapour pressure exceeds atmospheric pressure [7,9]. While the laser beam remains operating within the keyhole, the absorption increases due to the plasma within and the Fresnel reflections along the walls [10–13]. Multiple-reflections of the incident beam inside the keyhole cavity guide the focused beam, allowing it to propagate [14]. The front keyhole wall begins to incline and finally, a quasi-stationary maximum inclination angle is reached, typically around 0.2–0.3 s after the beginning of laser

* Corresponding author. Tel.: +44 0207882 7620.
E-mail address: r.castrejonpita@qmul.ac.uk (J.R. Castrejón-Pita).

http://dx.doi.org/10.1016/j.jmapro.2015.10.002

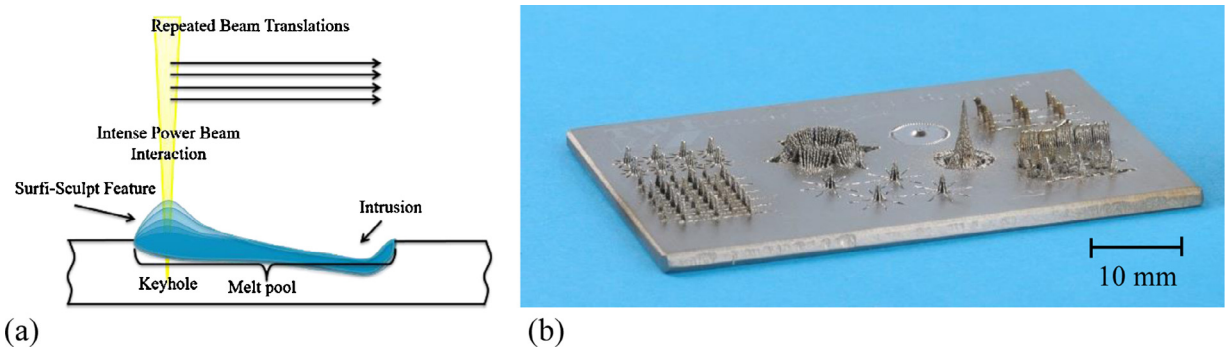

Fig. 1. (a) Surfi-Sculpt production, (b) example of range of Surfi-Sculpt features that can be produced for various applications.

irradiation [14], whilst the rear wall angle continuously fluctuates [10]. The melt flow around the keyhole exceeds the laser traverse speed by 2.5–10.0 times due to constriction between the cavity sides and the remaining solid material [15,16]. In fact, the flow around the keyhole includes a horizontal flow, a radial flow due to the thermocapillary effect (Marangoni flow) and a radial flow from vapour friction of the vapour flow [17]. In general, the local vaporisation causes an increase in the vertical momentum [5,9,18,19], which causes a projecting liquid filament to form when a supercritical flow rate is reached [20]. As a consequence, the liquid filament characteristics are influenced by the laser parameters and the processing speed, which in turn determine the hydrodynamic stability of the keyhole.

Strong melt fluctuations at the keyhole exit have previously been depicted and observed in literature [5,8,9,21–26] and are described as near-surface turbulent flows. The action of the vapour recoil pressure causes the melt layer on the front keyhole wall to regularly be removed forming moving liquid "shelves", these have been observed inside the keyhole [8,21,27]. Other fluctuations include bulges on the rear keyhole wall that are produced by an imbalance from recoil, hydrostatic and fluid dynamic pressures in addition to other instabilities such as thermo-capillary, Kelvin-Helmholz and, in particular, Rayleigh-Taylor [5,21].

At high laser transverse speeds a stagnation point of increased pressure forms behind the keyhole causing destabilisation of the melt pool surface and a formation point for a projecting liquid filament [28]. Higher processing powers increase the vapour recoil pressure, causing both a less regular melt flow and also increased vertical melt flow [9]. A similar protrusion has been observed to move upward with the flow of molten metal and accumulate to form a swelling behind the keyhole [5]. It is thought that these dynamics are caused by the collision of the upward flow and the downward flow due to surface tension and hydrostatic pressure [5].

The liquid filament of melt flow is thought to become fixed as a protrusion due to surface tension pinching the liquid filament and then solidifying to form a permanent feature. Repeated swipes of the laser with corresponding movement of molten material build up the surface feature.

1.3. Jet observations in welding

The formation of liquid filaments (jets) is non-steady due to the unstable vapour pressures within the keyhole. Maximum jet lengths have been reported to exceed the melt pool length just below the surface by 2–3 times [23]. The keyhole dynamics, the elongation and corresponding aspect ratio of the liquid filament become critical in the formation of spatter droplets [23]. This mechanism is shown schematically in Fig. 2.

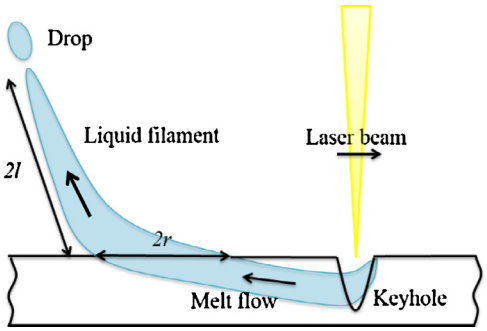

Fig. 2. Description of the boiling at the keyhole and momentum flow of an accelerating melt before necking and drop ejection.

Fig. 2 shows a rising liquid filament, fed by the flow around the keyhole, breaking into drops due to a balance of momentum and energy [9]. Melt ejection at the beginning of a laser interaction (within the first 3 ms), has previously been observed [24]. Four behavioural modes have been identified based on processing conditions including power, speed and laser beam focal position producing different formations of melt flow and filament breakup [9].

The flow of melt, the formation of the liquid filament and the solidification of the feature has been discussed by Fabbro [29]. It has been proposed that at high welding speeds, with rearward inclined keyholes, the ejected vapour plume intercepts the top of the melt pool along the keyhole rear wall. This collision elongates the keyhole aperture preventing the generation of a single melt wave, but instead oscillates the melt pool. Local pressure induced by the impact generates a side flow, directed towards the welding direction, which collides with the two main side flows coming from the keyhole front wall. These two melt jets are observed on the sides of the seam after solidification. Induced melt flow then dominates and can generate the humping regime, with severe undercuts. At rapid travel speeds a long narrow pool "tail" has been observed and is associated with welding discontinuities such as ropey bead, undercut and humping [30].

The "moving shelves" phenomenon previously described has, been attributed to bursts of vapour pressure in the melt volume. Pressure bursts occur when the Peclet number, *Pe*, exceeds a critical value. Peclet number defines the relation between mass and energy transport and is defined as $Pe = vD/\alpha$, where D is the laser beam diameter, v is the characteristic velocity, taken as the laser translation velocity and α is the thermal diffusivity [21]. A higher Peclet number corresponds to an elongated keyhole due to greater convective heat transfer [16,21,31–33]. If $Pe > 3$ the flow separates on the downstream side of the keyhole and two eddy flows are formed at the melt pool boundary [22,31]. This leads to the

Please cite this article in press as: Earl C, et al. The dynamics of laser surface modification. J Manuf Process (2015), http://dx.doi.org/10.1016/j.jmapro.2015.10.002

formation of a narrow high-speed jet at the centre line behind the keyhole [22,32].

The critical Peclet number for drop formation is $Pe \gg 1$, where the critical laser translation speed is:

$$v_c < 4\sqrt{2}\frac{\alpha}{D}\left(\ln\frac{q}{v}\right)^{0.5}, \quad (1)$$

and q is the laser power [21].

Rayleigh's liquid breakup model has been used to predict the liquid filaments behaviour by considering that naturally-occurring surface perturbations grow on liquid filaments until they cause breakup. Under this model, the breakup length (L_b) can be calculated from laser processing parameters by incorporating the molten material surface tension [30], this is:

$$L_b = \frac{12v_z}{\sqrt{(\sigma/\rho D^B)}}, \quad (2)$$

where v_z is taken as the laser translation velocity, σ is the surface tension of the molten liquid and ρ is the density of the liquid metal.

High-speed imaging of filament creation during laser processing in this work suggests that these filaments break up before they solidify. Therefore, standard liquid filament characterisation techniques can be applied in order to further understand the breakup behaviour.

1.4. Jet characterisation

Capillary instability and the breakup dynamics of liquid filaments has been observed and extensively studied in numerous fields since Rayleigh and Plateau [34–36]. Diverse numerical and theoretical models have been used to predict whether a filament of liquid will breakup into small droplets or condense into a single large drop. Experimental and numerical parametric studies exploring the stability of jets have demonstrated that the stability of long viscous filaments could be solely determined by two dimensionless groups; the aspect ratio, Γ, and the Ohnesorge number, Oh:

$$\Gamma = \frac{1}{r} \quad (3)$$

$$Oh = \frac{\mu}{\sqrt{\rho r \sigma'}}, \quad (4)$$

where $2l$ is the filament length, r is the initial filament radius and μ is the liquid viscosity [37,38]. The Ohnesorge number is the ratio between the viscous and the capillary timescales and provides an indication of the relative importance of these effects [39]. Generally speaking, surface tension dictates filament dynamics at low Ohnesorge numbers, while viscous forces drive behaviour at high Ohnesorge numbers [39]. It has been demonstrated that for low Ohnesorge numbers, $Oh < 0.01$, a critical aspect ratio $\Gamma_c = 6.0 \pm 1.0$ exists below which the filament does not breakup but collapses into a single drop [39,40]. This critical aspect ratio appears to be a universal lower boundary as no breakup has ever been observed for shorter filaments. The breakup of longer filaments at $Oh \ll 1$ is often called end pinching [35]. For $Oh \ll 1$, viscosity is not dominant, the dynamics are dominated by surface tension and the thinning rate of the filament is likely to follow a potential law until the point of break up [38]. In contrast, viscosity and surface perturbations or instabilities play a role for long filaments of higher Ohnesorge numbers [38]. Rayleigh-Plateu instabilities are the cause of breakup for long filaments. Linear analysis predicts that the most unstable perturbation (the fastest growing) has a wavelength λ of [41]:

$$\lambda = \frac{\sqrt{2+\sqrt{18}Oh}}{2\pi r}, \quad (5)$$

The growth rate of this perturbation is [38]

$$\beta = \frac{1}{\sqrt{2}}\left[\frac{1}{2+\sqrt{18}Oh}\left(1-\frac{1}{2+\sqrt{18}Oh}\right) + \frac{9}{2}Oh^2\left(\frac{1}{2+\sqrt{18}Oh}\right)^2\right]^{1/2} - \frac{3}{2}Oh\left(\frac{1}{2+\sqrt{18}Oh}\right), \quad (6)$$

and the time at which the filament breaks up by this instability can be approximated by

$$t_b = \frac{1}{\beta}t_c \ln\left(\frac{r}{\varepsilon}\right), \quad (7)$$

where t_c is the capillary time ($t_c^2 = \rho r^3/\sigma$) and ε is the initial amplitude of the disturbance [38,42]. For an instability to exist and produce the pinch-off, the viscous effects must be small enough to permit their growth and the length of a filament needs to be longer than λ.

In summary, long liquid filaments can breakup by two mechanisms, i.e. by end pinching and/or by Rayleigh-Plateu instabilities. The fate is determined by the initial conditions, i.e. initial aspect ratio, the properties of the fluid and whether instabilities have enough time to grow and produce breakup.

In this paper, high-speed imaging has been used to observe and record the production of surface features by laser processing. The obtained images show that during this process a liquid jet of molten metal is formed. A parametric study shows that the length of these filaments depends on the processing speed and power. Accordingly, the length and stability of the filament determines the size of the obtained surface feature.

2. Methodology

2.1. Laser processing

A single mode fibre laser YLR-1000-SM was used for all experiments (IPG Photonics Inc., USA). The laser produced a rated maximum output power of 1 kW at the central emission wavelength of 1064 nm. The beam caustic produced using the focusing system gave a minimum beam radius of 23.15 μm and a beam parameter product (BPP) of 0.50 mm mrad. The measured Rayleigh length was 1.18 mm. The laser was scanned across the target material using an ARGES fibre Elephant scanner (50 mm aperture) using a focussing lens and a galvonometer driven mirror system. An argon (Pureshield argon to BS EN 439) atmosphere was established by placing the processing material in an open-top chamber running with a continuous argon flow rate of 16 l/min at a pressure of 350 kPa. Under these conditions, an oxygen content of 0.07% was achieved to minimise oxidation. During experiments, laser power and scan speed were varied. The swipe length was set to 3 mm as had previously been shown to produce surface features and the focal point placed at the surface of the target [43]. The delay time between laser swipes was set to 20 ms.

2.2. High-speed imaging equipment

High-speed imaging was carried out using a Phantom V710 camera set at 40,000 fps with an exposure time of 24.64 μs. The camera was coupled to a 12× Navitar lens producing a resolution of 2 μm/pixel. The field of view was illuminated by two 500 W pulsed Cavilux HF lasers operating at an 810 nm wavelength. The illumination lasers were positioned slightly above and to either side of the camera. A white nylon block was placed behind the processing area to produce an adequate contrast background. A 1.00 μm band-pass filter was placed in front of the high-speed camera to enhance the quality of the images by removing the processing laser wavelength.

Please cite this article in press as: Earl C, et al. The dynamics of laser surface modification. J Manuf Process (2015), http://dx.doi.org/10.1016/j.jmapro.2015.10.002

Table 1
Material physical property data used for calculations.

Material	Stainless Steel 304	Ti–6Al–4V	Aluminium 5000
Density of liquid, ρ (kg m^{-3})	7000 [33]	4420 [44]	2357 [45]
Surface tension, σ (liquid in Argon atmosphere) (N m^{-1})	1.169 [46]	1.460 [47]	0.876 [48]
Thermal diffusivity of liquid (m^2 s^{-1})	51.79×10^{-5} [33]	1.07×10^{-5} [33]	5.09×10^{-5} [45]
Dynamic viscosity (kg m^{-1} s^{-1})	0.007 [33]	0.005 [33]	0.003 [44]

The Cavilux illumination focusing lenses were positioned approximately 150 mm away from the feature in order to achieve a sharp image.

2.3. Materials and material preparation

Experiments were performed on the following materials: 304 stainless steel, Ti–6Al–4V and Aluminium 5000 series all of which are commonly used in industrial applications. Material properties are shown in Table 1.

The materials were cut into samples of 10 mm by 50 mm and all edges were de-burred. The thickness of the materials was as follow: Stainless steel 304 = 6 mm, Ti–6Al–4V = 2.6 mm and aluminium = 1.2 mm. The Stainless steel 304 surface was finished by grinding to a 2500 paper while Ti–6Al–4V and aluminium surfaces were prepared by scourer scrubbing. Samples were cleaned with acetone to remove any grease or deposits.

2.4. Filament measurement

The liquid filament aspect ratios were measured using the Phantom Camera Control Software. Measurements were taken over the first ten frames at the start of processing and the frame with the maximum filament length was selected to represent each particular processing condition.

3. Results

3.1. Relation of Surfi-Sculpt to filament breakup

Examples of high-speed images of initial processing swipe are shown in Table 2. The experiments at high processing speeds show a vertical liquid column being formed behind the keyhole which subsequently breaks into droplets. As can be observed in Table 2, the filament length, volume and ejection angle increases with the increased processing speed.

Table 2
High-speed imaging of the surface feature processing of Ti–6Al–4V at a range of laser transverse speeds. In these experiments, the laser power was set at 1 kW.

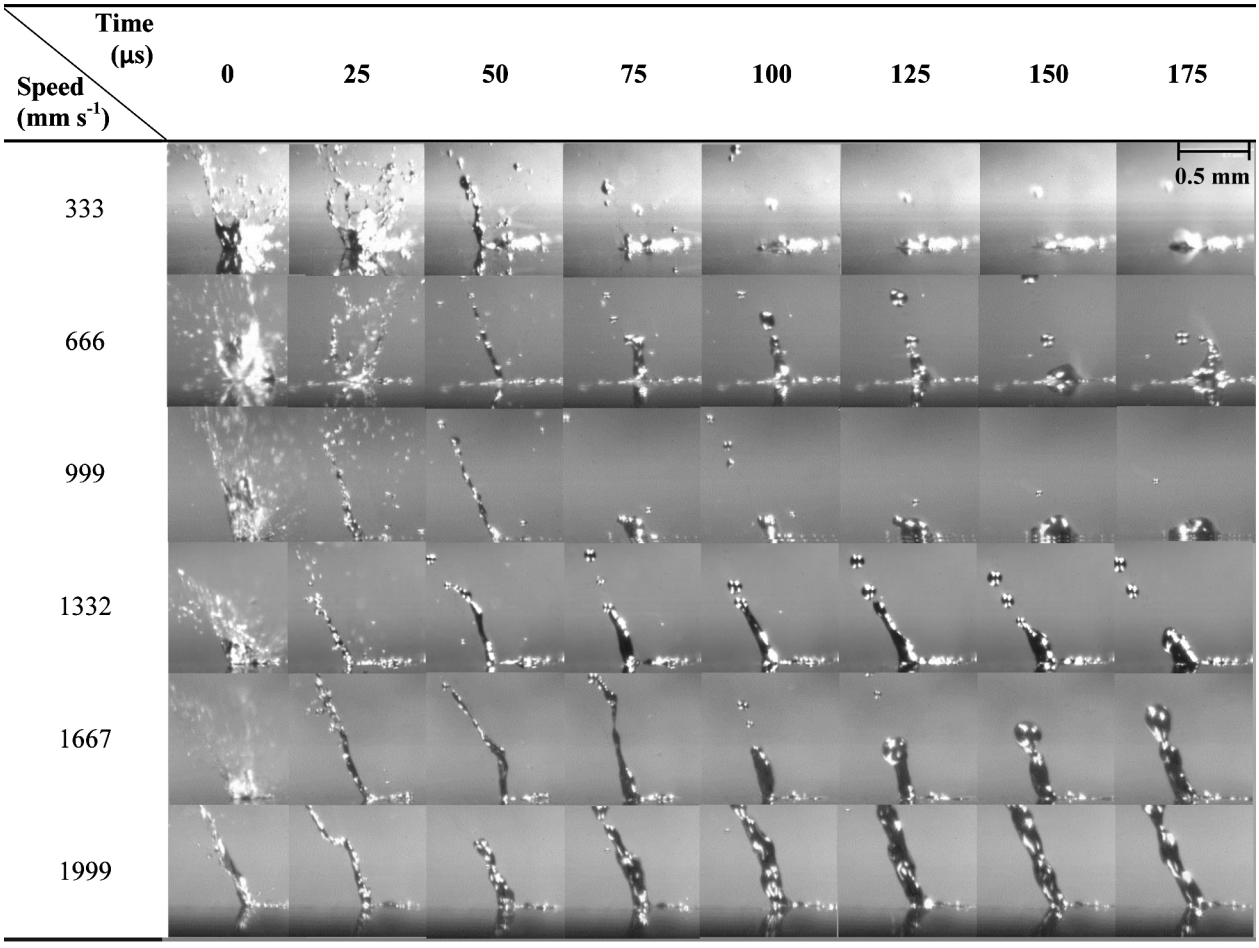

Please cite this article in press as: Earl C, et al. The dynamics of laser surface modification. J Manuf Process (2015), http://dx.doi.org/10.1016/j.jmapro.2015.10.002

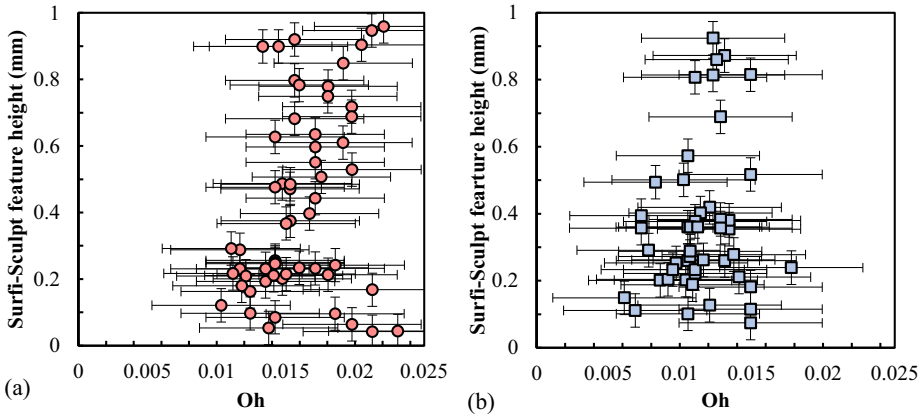

Fig. 3. *Oh* against solidified Surfi-Sculpt feature height (a) Stainless steel 304 and (b) Ti–6Al–4V.

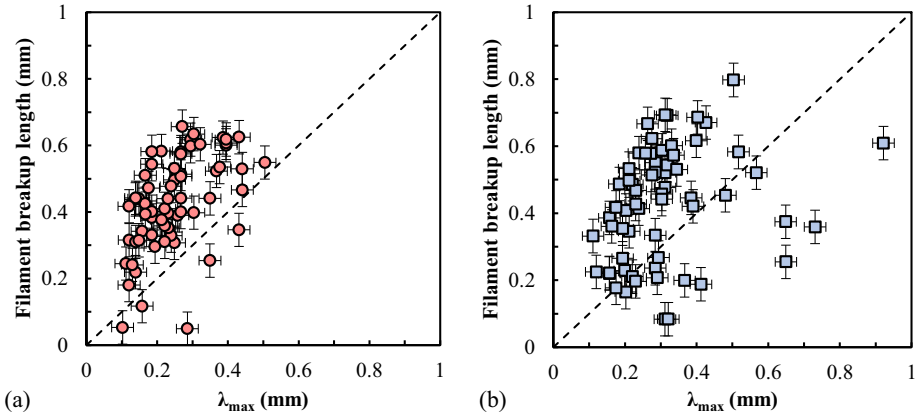

Fig. 4. Comparison of the most unstable perturbation wavelength to the filament breakup length ($2l$) (a) Stainless steel 304 and (b) Ti–6Al–4V.

From Table 2, it can be seen that most droplets break away at the end of each filament when a threshold length is exceeded. This is particularly clear for speeds of 13,332 mm s^{-1} or above, where a continuous filament is formed and stable for 100 μs, while droplets are detached from the filament's end. For higher speeds, >1666 mm s^{-1}, the filament also starts to breakup along its length indicating that this breakup is driven by Rayleigh instabilities. Table 2, also shows the early laser–substrate interaction is very unstable, producing short-lived fast spatter. A stable jet is only formed after 50 μs from the first laser–substrate interaction.

Previous studies have demonstrated that viscosity and inertia only become important once the filament necks below $h_{\min} = rOh^2$ [40,49]. While it has been considered that inertial effects are present within the filament from the driving force of the keyhole cavity flow, the low Ohnesorge numbers of these systems indicate that viscous effects are not important in the thinning and breakup.

Under experimental conditions, Fig. 3, these filaments exist within the range of $0.050 < Oh < 0.025$, and as seen from Table 2, filament radii are within the range 0.04 mm < r < 0.11 mm. These conditions indicate that viscous effects only start to play a role on the thinning once the neck has reduced to 300 nm which is around the diffraction limit of the optical system. As a consequence, the thinning process observed by the imaging can be described as an inviscid liquid for all the conditions studied here.

Being an inviscid process, the breakup at the end of the filament is likely to occur by end-pinching. However, breakup at the middle of the filament can occur due to the growth of Rayleigh-Plateau instabilities [38]. As previously explained, if the filament length is longer than the most unstable perturbation wavelength and the filament exists long enough for that instability to grow, then the filament will breakup due to Rayleigh-Plateau instabilities. Fig. 4 shows that, for most filaments, the maximum instability wavelength is shorter than the filament breakup length and therefore Rayleigh-Plateau instabilities could exist, grow and consequently produce breakup. Within our experimental conditions, capillary times were in the range of 2.3 μs < t_c < 57.6 μs which in turns produce breakup times in the range of 32.4 μs < t_b < 766.1 μs for initial instabilities of ε/r of 0.01. As expected, higher initial instabilities only produce faster breakup times, i.e. 16.2 μs < t_b < 383.1 μs for $\varepsilon/r = 0.1$, and 4.8 μs < t_b < 115.3 μs for $\varepsilon/r = 0.5$. These predicted breakup times are within the time scales observed under the experimental conditions, confirming that Rayleigh instabilities could cause the breakup along the jet.

It has been demonstrated that under these experimental conditions the filaments produced during the processing time can breakup by end pinching and/or by surface instabilities. As previously discussed, parametric studies of the breakup of liquid filaments have demonstrated that a critical initial aspect ratio of 6.0 ± 1.0 exists below which a liquid filament will not breakup, irrespective of the *Oh* number [39]. Within the conditions explored in these experiments, with one exception only, the filaments studied here with surface features >0.5 mm in height, have aspect ratios greater than the critical value, Fig. 5.

It is important to notice that previous analyses have only dealt with static filaments with no stretching, contraction or significant inner dynamics. This limitation may explain the data point that does not follow the predicted behaviour in Fig. 5, i.e. the inner

Please cite this article in press as: Earl C, et al. The dynamics of laser surface modification. J Manuf Process (2015), http://dx.doi.org/10.1016/j.jmapro.2015.10.002

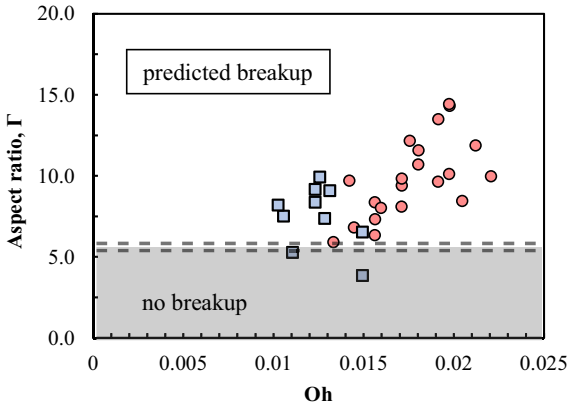

Fig. 5. Experimental results for stainless steel (red circles) and Ti–6Al–4V (blue squares) in terms of the Ohnesorge number and the filament aspect ratio. Under the experimental conditions explored here, all the filaments broke up and feature height was >0.5 mm in height. Critical initial aspect ratio from [38]. (For interpretation of the references to color in this figure legend, the reader is referred to the web version of this article.)

dynamics of these filaments may be important enough to alter the breakup behaviour.

3.2. Feature characterisation

Tall feature heights from a minimal number of passes are highly desired in laser surface modification processes because they reduce the time of manufacturing and make a more efficient use of the substrate material.

The experimental data on this work shows that the geometry of the protruded liquid filament produced during processing time determines the height of the final feature. The relation between the filament aspect ratio and filament height is shown in Fig. 6. The height of the solid features produced was measured using a micrometre, with this being measured relative to the material surface. Results indicate that filament aspect ratios above the critical value for breakup of 6, as shown by the dotted line in Fig. 6, increased the feature height. This suggests that the filament must be unstable enough to breakup to form features. The results show that for increased filament length beyond this value there was no further increase in feature height. Feature heights taller than 0.5 mm were deemed successful features for manufacturing.

Fig. 7 shows the dependency of the feature height formed by the surface modification process in terms of the liquid filament lengths over 0.2 mm for Stainless steel 304 and 0.3 mm for Ti–6Al–4V.

As described elsewhere, the laser processing parameters influence the keyhole dimensions which in turn affects the melt flow and keyhole stability. The flow within the keyhole then affects the behaviour of the filament and so the process of feature creation. The relationship between processing parameters and filament length is shown in Fig. 8. These results show the dependency of filament length in terms of the laser power and the speed of processing. When considering the relation of process parameters to feature production, both Stainless steel 304 and Ti–6Al–4V produced relatively taller features at a line energy (Power/speed) of 600 Ws m^{-1}.

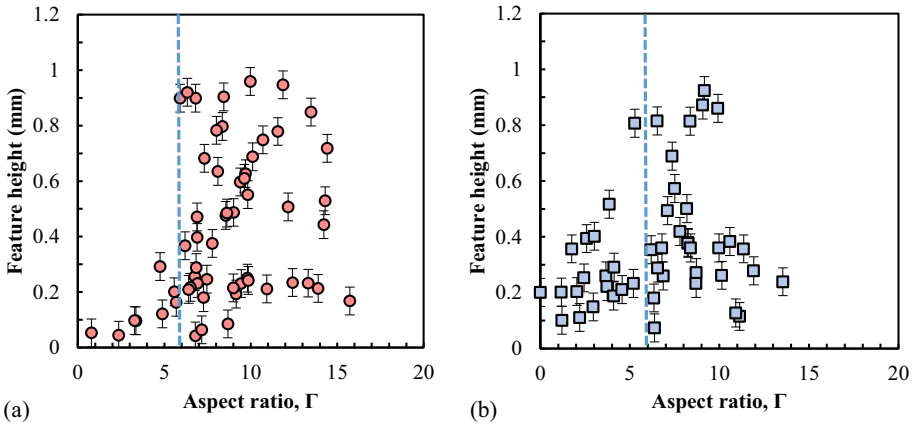

Fig. 6. Filament aspect ratio calculated from jet measurments against surface feature height, (a) Stainless steel 304 and (b) Ti–6Al–4V.

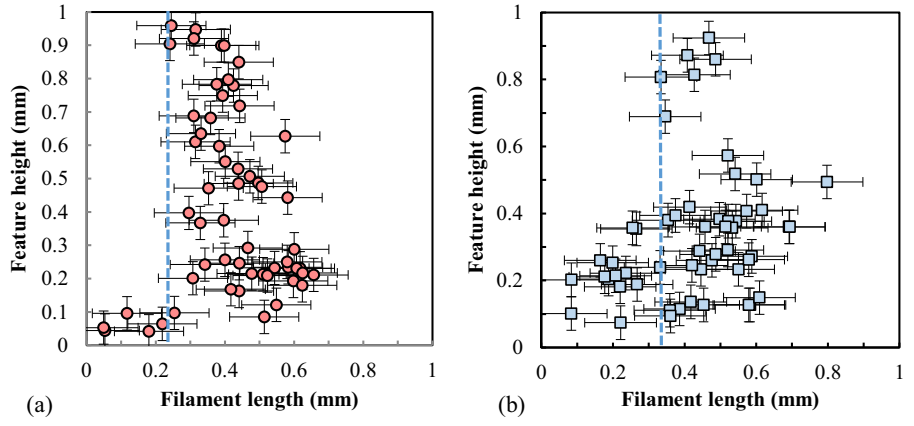

Fig. 7. Measured breakup length plotted against feature height for (a) Stainless steel 304 and (b) Ti–6Al–4V.

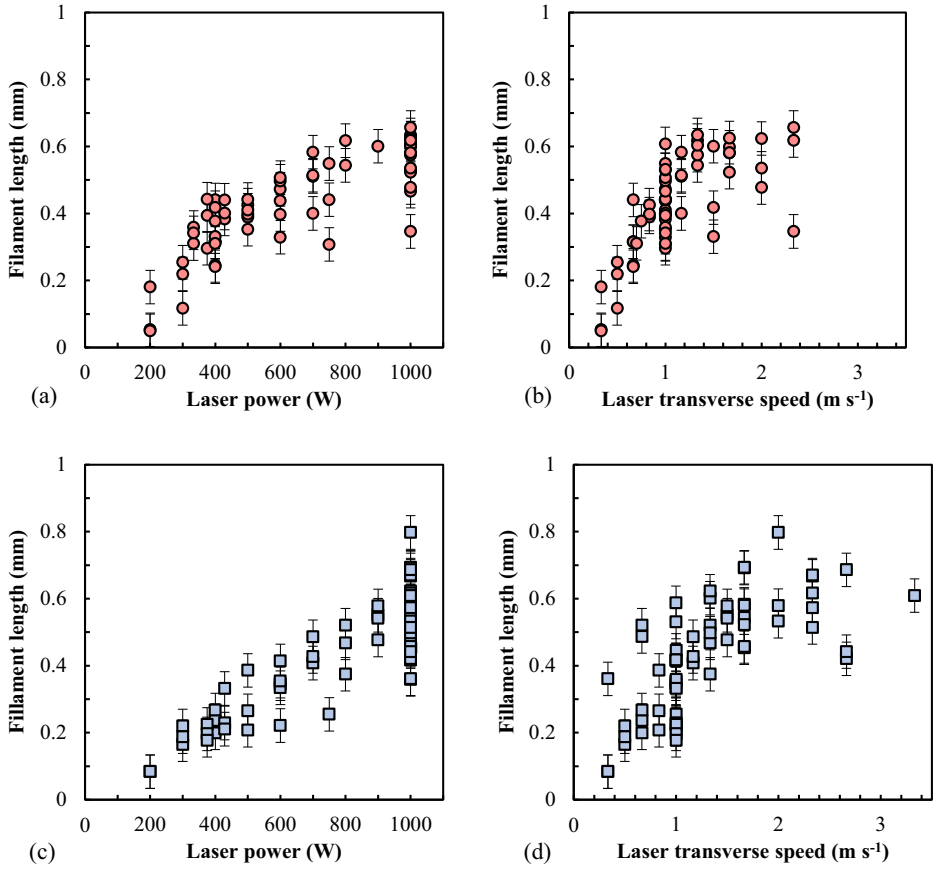

Fig. 8. Relation between processing parameters of power and speed and measured breakup length; (a) and (b) Stainless steel 304, (c) and (d) Ti–6Al–4V.

However, this is achieved with higher processing powers and speeds with Ti–6Al–4V than Stainless steel 304.

The filament length has also been compared to the predicted breakup length calculated from Eq. (2). This comparison is shown in Fig. 9. These results show that Eq. (2) tends to underestimate the size of filament breakup length. This discrepancy could be produced by practical limitations, such as an error in laser alignment as a focussing error could cause the spot size to be slightly larger than the minimum laser spot size.

4. Predicting Surfi-Sculpt

Based on the results presented in this paper, it should be possible to predict the onset and processing parameters for laser surface feature production. In particular, the importance of the critical aspect ratio in identifying the operating region required for surface feature formation. The ideal processing parameters can be determined by just considering the material properties, in particular molten surface tension in the given gas environment. The analysis is based on predicting the processing conditions that produce a filament with the minimal critical aspect ratio so it breaks up to efficiently produce a tall surface protrusion. The corresponding filament length, l, can be calculated from the aspect ratio, Eq. (3), taking r as the laser spot radius. The critical filament length can then be used to find minimum laser translation velocity, v_z, Eq. (2), using material values from Table 1 and atmospheric surface tension is taken into account. To find the minimum processing power, first the speed of sound for the material is calculated, v_c, according to Eq. (1). The ratio of power to speed used to calculate the initial values of v_c, was taken as the optimum processing line energy of 597 Ws m^{-1}. This was identified when developing the fit of this model and is close to the previously experimentally found optimum of 600 Ws m^{-1}. Table 3 shows the processing parameters calculated for the materials investigated and predicts the processing conditions for aluminium 5000, Fig. 10.

Table 3
Values for predicting processing parameters for laser surface modification in Stainless steel 304, Ti–6Al–4 V and Aluminium 5000.

	Stainless steel 304	Ti–6Al–4V	Aluminium 5xxx
Critical aspect ratio, Γ_c	5	5	5
Filament length, l (mm)	0.23148	0.23148	0.23148
Minimum processing speed, v_z (m s^{-1})	0.79	1.11	1.18
Speed of sound for material, v_c (m s^{-1})	1.60	3.31	15.73
Minimum processing power, q (W)	472.44	664.44	704.79

Maximum processing conditions can be estimated using the same method but with a higher critical aspect ratio, e.g. 10 from Fig. 6. Validation of the processing parameters, showing a close correlation to experimental results, is show in Fig. 10.

Fig. 11 shows the experimental results for Aluminum 5xxx and confirms that the onset for the creation of tall laser Surfi-Sculpt features is achieved once the filament aspect ratio achieves its unstable length. Surface tension is the main factor influencing filament breakup and thus the most important factor controlling Surfi-Sculpt production. It is important that the jet produced is wide enough to enable higher processing powers and speeds to be employed to produce it, moving a greater volume of material.

Please cite this article in press as: Earl C, et al. The dynamics of laser surface modification. J Manuf Process (2015), http://dx.doi.org/10.1016/j.jmapro.2015.10.002

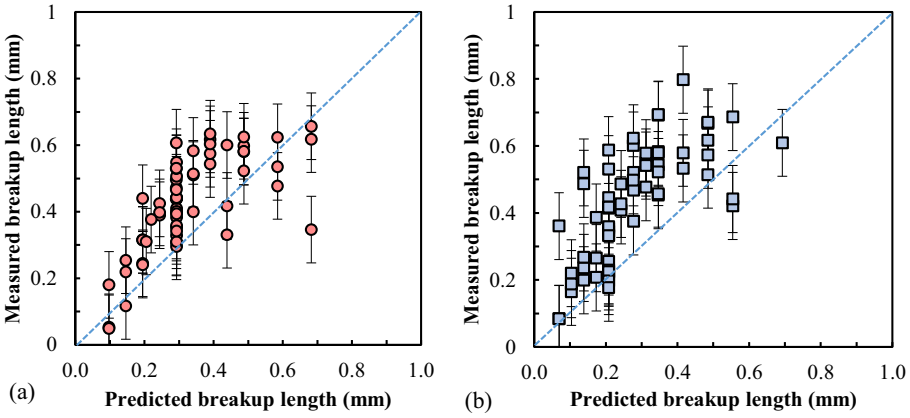

Fig. 9. Predicted jet breakup length plotted against the measured breakup for (a) Stainless steel 304 and (b) Ti–6Al–4V.

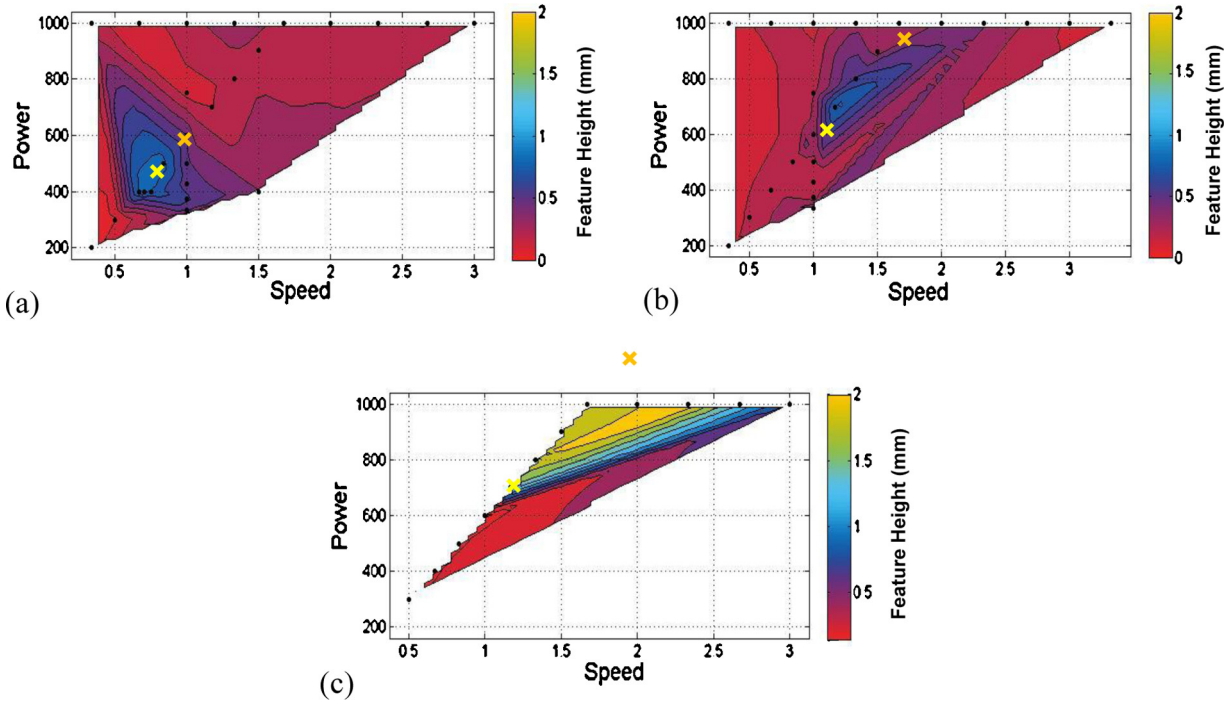

Fig. 10. Predicted processing parameters (yellow cross) overlaid on laser Surfi-Sculpt production experimental results for (a) Stainless steel 304, (b) Ti–6Al–4V and (c) Aluminium 5000 series. (For interpretation of the references to color in this figure legend, the reader is referred to the web version of this article.)

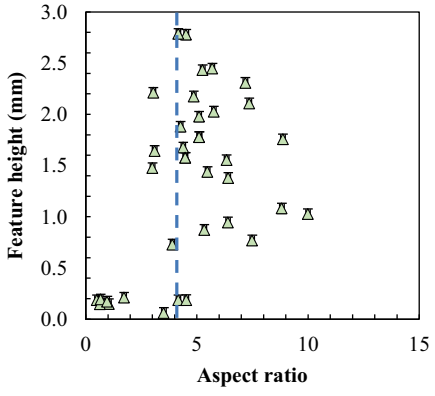

Fig. 11. Aspect ratio obtained from experimental jet measurments against Surfi-Sculpt feature height for Alunminim 5000 series.

5. Discussion

The jet behaviour seen in this surface modification technique is in agreement with that described by Kaplan and named as mode II [9]. This behaviour is observed despite operating at a much lower power level in this work, but with a smaller spot size and higher processing speed, suggesting that the operating mode is a function of power density [9]. In contrast, at low speeds, the filament is not stable; it rapidly breaks up and heavy spatter is observed. This behaviour has been called mode III jetting in Kaplans work [8]. It is therefore thought that the operating mode is a function of power density as well as process speed.

As hypothesised, it is shown that with longer jet lengths, more material is available to create a feature. However, if the filament length is too long this results in larger droplets breaking up as spatter making less material available for feature formation.

The material-specific laser absorption coefficient was considered for the equations to calculate v_c. However, adding the

coefficient would be cancelled out when calculating the input power, q. The processing power is the value that would be input into the laser and therefore interaction absorption does not need to be considered for practical purposes. The absorption for a keyhole would also be very close to 100% (0.98) and would therefore not affect strongly any results [12].

When considering the application of these findings to multiple swipes it is observed that the jets are still formed during subsequent swipes. However, with feature formation occurring there would be a physical interaction of the jet with the existing feature. It is expected that this would have several effects. Firstly, the filament is likely to be bounded to the feature, decreasing the surface area [50], increasing the surface tension force and enhancing the earlier onset of filament breakup. This helps to explain the exponential decrease in additional feature height with increasing number of swipes [3,4]. Secondly, the texture of the formed feature surface would introduce a shear stress opposing the melt momentum and would also influence capillarity effects – either positively or negatively. For these reasons the model cannot be applied when producing features in formations of close proximity, <0.25 mm, where capillary action can act (e.g. star formations, Fig. 1b). With progressive swipe repeats, thermal energy will build up within the substrate. It is hypothesised that an increase in substrate temperature would increase the melt pool width and keyhole dimension. This would in turn affect the expelled jet dimensions and decrease the jet aspect ratio, reducing the prospect of the onset of surface feature production. If this occurs, increasing the processing speed may counteract the increase in jet diameter by increasing the jet length. Increasing the processing power is undesirable in this situation as this would increase the jet diameter and increase heating of the substrate further.

It is thought that the line energy requirement of 597 $\mathrm{W\,s\,m^{-1}}$ is related to the keyhole penetration depth or aspect ratio [8], as this relation has been noted in equations related to laser processing such as the distance between humps, d_h, when processing at speeds when the humping phenomenon is observed:

$$d_h = \sqrt{\frac{\rho}{\nu}},$$

from [51].

As previously mentioned, the operating mode is a function of power density as well as processing speed. It is therefore unsurprising that line energy is so important to the feature production mechanism. It is particularly interesting that this value is constant and yet the values for power and speed for optimum processing vary depending on the material. It is thought that this is due to the conduction distribution varied by not only the materials used, but also the power and speed. This affects the ratio of heat distribution as well as the size and shape of the keyhole influencing the fluid motion at the surfaces. In particular, if the depth of the melt exceeds the weld pool radius, as is predominant with keyhole welding, then 'volumetric' oscillations can be assumed, rather than capillary waves [24]. The oscillation frequency is also highly sensitive to processing parameters as these influence the initial melt mass [24]. This importance of how energy is applied rather than the quantity of energy has been noted in other forms of laser processing [52].

If different laser systems are to be used it is hypothesised that the aspect ratio criteria should ensure that the effects of the laser spot size are incorporated.

6. Conclusion

It has been established that there is a strong relation between laser surface feature production and jet stability and breakup. High-speed imaging has been used to show that filaments of molten material are produced due to the keyhole formation and dynamics. Analysis of jets has shown that the breakup mechanism is a limiting factor of feature production and that this is driven by surface tension and surface instabilities. For the onset of laser surface modification it has been found that a critical aspect ratio of 6.0 ± 1.0 must be achieved. Irrespective of the material and its properties. Using jet breakup theory and spatter production equations, the feasibility of predicting laser processing parameters for surface feature production in Stainless steel 304, Ti–6Al–4V, and Aluminium 5000 series has been demonstrated.

Acknowledgments

This work is funded by the Engineering and Physical Sciences Research Council (EPSRC) CASE award number NMZM/162 RG61816 and TWI Ltd. The authors would like to thank the EPSRC Engineering Instrument Loan Pool and Peter Anthony for the loan of the high speed imaging camera and illumination system. Also, thanks to Wen-Kai Hsiao for the loan of the imaging lens. JRCP acknowledges the support from the EPSRC (project number EP/H018913/).

References

[1] Buxton AL, Dance BGI. Surfi-sculpt – revolutionary surface processing with an electron beam ISEC Cong. St. Paul, MN, USA: ASM International; 2005.
[2] Blackburn J, Hilton P. Producing surface features with a 200 W Yb-fibre laser and the surfi-sculpt® process. Phys Proc 2011;12:529.
[3] Blackburn JE, Hilton PA. The generation of autogeneous surface features using a low power laser beam. Anaheim, CA, USA: ICALEO; 2010. p. 1704.
[4] Earl C, Hilton P, O'neill W. Parameter influence on surfi-sculpt processing efficiency. Phys Proc 2012;39:327.
[5] Zhang MJ, Chen GY, Zhou Y, Li SC, Deng H. Observation of spatter formation mechanisms in high-power fiber laser welding of thick plate. Appl Surf Sci 2013;280.
[6] Amara E, Fabbro R. Modeling of humps formation during deep-penetration laser welding. Appl Phys A 2010;101.
[7] Beyer IE. Plasmaabsorption Schweißen mit laser. Springer; 1995. p. 49–77.
[8] Golubev VS. Laser welding and cutting: recent insights into fluid-dynamics mechanisms. In: Proc. SPIE 5121, laser processing of advanced materials and laser microtechnologies. 2003. p. 1–15.
[9] Kaplan A, Westin E, Wiklund G, Norman P. Imaging in cooperation with modeling of selected defect mechanisms during fiber laser welding of stainless steel. Temecula, CA, USA (LIA): ICALEO; 2008. p. 789.
[10] Fabbro R, Chouf K. Keyhole modeling during laser welding. J Appl Phys 2000;87.
[11] Schuöcker D. High power lasers in production engineering. London Imperial College Press; 1999.
[12] Steen WM. Laser materials processing. Springer-Verlag; 1991.
[13] Jin X, Zeng L, Cheng Y. Direct observation of keyhole plasma characteristics in deep penetration laser welding of aluminum alloy 6016. J Phys D: Appl Phys 2012;45.
[14] Fabbro R, Slimani S, Coste F, Briand F. Study of keyhole behaviour for full penetration Nd–Yag CW laser welding. J Phys D: Appl Phys 2005;38.
[15] Berger P, Hügel H, Hess A, Weber R, Graf T. Understanding of humping based on conservation of volume flow. Phys Proc 2011;12.
[16] Behler K, Schäfer P. Melt pool dynamics in high speed welding with modern high power solid state lasers, vol. 2205. Miami, FL (LIA): ICALEO; 2005.
[17] Sudnik W, Radaj D, Breitschwerdt S, Erofeew W. Numerical simulation of weld pool geometry in laser beam welding. J Phys D: Appl Phys 2000;33.
[18] Kaplan A, Powell J. Spatter in laser welding. J Laser Appl 2011;23.
[19] Matsunawa A, Seto N, Kim J-D, Mizutani M, Katayama S. Dynamics of keyhole and molten pool in high power CO_2 laser welding. Proc SPIE (Osaka, Japan) 2000;3888:34–45.
[20] Savage W, Nippes E, Agusa K. Effect of arc force on defect formation in GTA welding. Weld J 1979;58.
[21] Kumar N, Dash S, Tyagi AK, Raj B. Hydrodynamical phenomena in the process of laser welding and cutting. Sci Tech Weld Join 2007;12.
[22] Mahrle A, Schmidt J. The influence of fluid flow phenomena on the laser beam welding process. Int J Heat Fluid Flow 2002;23.
[23] Seefeld T. Chances and challenges processing with high brightness lasers. Anaheim, CA, USA (LIA): ICALEO; 2010.
[24] Semak V, Hopkins J, Mccay M, Mccay T. Melt pool dynamics during laser welding. J Phys D: Appl Phys 1995;28.
[25] Fishburn JM, Withford MJ, Coutts DW, Piper JA. Study of the fluence dependent interplay between laser induced material removal mechanisms in metals: vaporization, melt displacement and melt ejection. Appl Surf Sci 2006;252.

Please cite this article in press as: Earl C, et al. The dynamics of laser surface modification. J Manuf Process (2015), http://dx.doi.org/10.1016/j.jmapro.2015.10.002

[26] Fishburn JM, Withford MJ, Coutts DW, Piper JA. Study of the interplay of vaporisation, melt displacement and melt ejection mechanisms under multiple pulse irradiation of metals. Appl Surf Sci 2006;253.
[27] Zhang M, Chen G, Zhou Y, Li S. Direct observation of keyhole characteristics in deep penetration laser welding with a 10 kW fiber laser. Opt Express 2013;21:19997.
[28] Gratzke U, Kapadia PD, Dowden J, Kroos J, Simon G. Theoretical approach to the humping phenomenon in welding processes. J Phys D: Appl Phys 1992;25.
[29] Fabbro R, Slimani S, Coste F, Briand F. Analysis of the various melt pool hydrodynamic regimes observed during CW Nd-Yag deep penetration laser welding. FL, USA (LIA): ICALEO; 2007.
[30] Albright C, Chiang S. High speed laser welding discontinuities. Laser Materials Processing; 1988.
[31] Ye X-H, Chen X. Three-dimensional modelling of heat transfer and fluid flow in laser full-penetration welding. J Phys D: Appl Phys 2002;35.
[32] Mahrle A, Schmidt J, Weiss D. Simulation of temperature fields in arc and beam welding. Heat Mass Transfer 2000;36.
[33] Rai R, Elmer J, Palmer T, Debroy T. Heat transfer and fluid flow during keyhole mode laser welding of tantalum, Ti–6Al–4V, 304L stainless steel and vanadium. J Phys D: Appl Phys 2007;40.
[34] Rayleigh L. XVI. On the instability of a cylinder of viscous liquid under capillary force. Philos Mag 1892;34.
[35] Strutt JW, Rayleigh L. On the instability of jets. Tr. Mat. O-va; 1879.
[36] Yuen M-C. Non-linear capillary instability of a liquid jet. J Fluid Mech 1968;33.
[37] Van Elsen M, Al-Bender F, Kruth J-P. Application of dimensional analysis to selective laser melting. Rapid Prototyp J 2008;14.
[38] Driessen T, Jeurissen R, Wijshoff H, Toschi F, Lohse D. Stability of viscous long liquid filaments. Phys Fluids 2013;25.
[39] Castrejón-Pita AA, Castrejón-Pita J, Hutchings I. Breakup of liquid filaments. Phys Rev Lett 2012;108.
[40] Notz PK, Basaran OA. Dynamics and breakup of a contracting liquid filament. J Fluid Mech 2004;512.
[41] Chen AU, Notz PK, Basaran OA. Computational and experimental analysis of pinch-off and scaling. Phys Rev Lett 2002;88.
[42] Dong H, Carr WW, Morris JF. An experimental study of drop-on-demand drop formation. Phys Fluids 2006;18.
[43] Earl CL, Hilton PA. Towards an understanding of laser induced surfi-sculpt. Great Abington: TWI Ltd.; 2012.
[44] Gale WF, Totemeier TC, editors. Smithells metals reference book. Butterworth-Heinemann; 2003.
[45] Hatch JE. Aluminum: properties and physical metallurgy. ASM International; 1984.
[46] Wen J, Lundin C. Technical note: surface tension of 304 stainless steel under welding conditions. Weld J 1986;65.
[47] Zhu J, Kamiya A, Yamada T, Shi W, Naganuma K, Mukai K. Surface tension, wettability and reactivity of molten titanium in Ti/yttria-stabilized zirconia system. Mater Sci Eng A 2002;327.
[48] Saravanan R, Molina J, Narciso J, Garcia-Cordovilla C, Louis E. Surface tension of pure aluminum in argon/hydrogen and nitrogen/hydrogen atmospheres at high temperatures. J Mater Sci Lett 2002;21.
[49] Lister JR, Stone HA. Capillary breakup of a viscous thread surrounded by another viscous fluid. Phys Fluids 1998;10.
[50] Trefethen L. Film notes for surface tension in fluid mechanics. National Committee for Fluid Mechanics Films; 1969. p. 21610.
[51] Berger P, Hügel H, Hess A, Weber R, Graf T. Understanding of humping based on conservation of volume flow. Phys Proc 2011;12:232.
[52] Pangovski K, Sparkes M, Cockburn A, O'neill W, Peh Siong T, Dejiao L, et al. Control of material transport through pulse shape manipulation – a development toward designer pulses. Sel Top Quant Electron IEEE J 2014;20.

Please cite this article in press as: Earl C, et al. The dynamics of laser surface modification. J Manuf Process (2015), http://dx.doi.org/10.1016/j.jmapro.2015.10.002